RSC Advances

PAPER

View Article Online
View Journal | View Issue

Cite this: *RSC Adv.*, 2016, **6**, 75552

A strategy for the synthesis of cyclomatrix-polyphosphazene nanoparticles from non-aromatic monomers†

Zhangjun Huang,[a] Feng Zheng,[a] Shuangshuang Chen,[a] Xuemin Lu,[a] Cornelia Gertina Catharina Elizabeth van Sittert[b] and Qinghua Lu*[a]

Received 24th May 2016
Accepted 16th July 2016

DOI: 10.1039/c6ra13486f

www.rsc.org/advances

Cyclomatrix-polyphosphazenes (C-PPZs) are a new class of nanomaterials that have attracted significant interest owing to their unique inorganic–organic hybrid structure and tunable properties. The limited success that has been achieved in producing C-PPZs from non-aromatic organic monomers is ascribed to an insufficient understanding of their polymerization mechanism. In this work, by using a new strategy termed solubility-parameter-triggered polycondensation, we demonstrate experimentally and computationally that C-PPZs nanoparticle synthesis from non-aromatic monomers is feasible and solubility-parameter (SP)-dependent. The precipitation polycondensation of C-PPZ occurs once the solution SP is outside a critical SP range, while within the critical range only oligomers are detected from the reaction; this SP-dependent rule is applicable for C-PPZ oligomers from both aromatic and non-aromatic monomers. The upper/lower critical SP values increase with the increase of organic monomer hydrophilicity. The morphologies of C-PPZ products exist as clusters or nanoparticles when the reaction solvent SP is controlled below the upper critical SP or exceeds the lower critical SP, respectively. This theory presents a feasible way to predict and determine the precipitation polycondensation conditions and product morphology of any novel C-PPZ nanomaterial.

1 Introduction

Phosphazene-based polymers have shown great potential in their applications as biomaterials,[1–5] membranes,[6,7] solid electrolytes,[8–11] supporter for catalyst,[12–16] coating materials,[17,18] flame retardants,[19,20] and elastomers.[21–23] This class of polymers contain phosphorus and nitrogen alternating backbones and it is easy to introduce functional groups into the polymers by substituting the active chlorine atoms on each phosphorus atom. Their physicochemical properties can be regulated easily by changing various organic groups on the phosphorus center. Therefore, such organic–inorganic hybrid polymers possess a flexible molecular design and tunable material properties.[24,25] The most extensively studied phosphazene-based polymers are linear polyphosphazenes.[26,27] Industrial scale synthesis of linear polyphosphazene is achieved through the ring-opening polymerization of hexachlorocyclotriphosphazene (HCCP). Although this method can result in the synthesis of high molecular weight materials ($M_n \approx 10^6$ Da), it suffers from several deficiencies such as harsh synthesis conditions (250 °C in vacuum) and wide molecular weight distribution (PDIs ≈ 10). Several efforts have been made to overcome the problems of ROP method. On one hand, the "living" cationic polymerization method was developed to achieve polyphosphazene with narrow molecular weight distribution and complex architectures.[28–31] On the other hand, a new alternative class of polyphosphazenes, *i.e.*, cyclomatrix polyphosphazenes (C-PPZs), has emerged in the last decade as nanomaterials.[32] C-PPZs can be obtained easily and in large quantities by precipitation polycondensation from HCCP and organic monomers or polymers (diols/di-amines) as nanoparticles under ambient conditions. Phosphazene rings in the polymers are linked *via* exocyclic groups with organic monomers to form a highly crosslinked polymeric network.[33–38] However, the C-PPZs nanoparticles reported to date are majorly prepared from aromatic monomers, which have potential toxicity for bioapplications such as drug delivery, gene transfection, and embolic agents. Non-aromatic organic monomers with diamine are promising alternatives for the aromatic monomers, especially amino acid esters. Linear polyphosphazenes substituted by non-aromatic organic monomers have been proven to be biocompatible, biodegradable and their degradation products are non- or low toxic compounds, for

[a]*School of Chemistry and Chemical Engineering, The State Key Laboratory of Metal Matrix Composites, Shanghai Jiaotong University, Shanghai, P. R. China. E-mail: qhlu@sjtu.edu.cn*

[b]*Catalysis and Synthesis Research Group, Chemical Resource Beneficiation Focus Area, North-West University, Potchefstroom, South Africa*

† Electronic supplementary information (ESI) available. See DOI: 10.1039/c6ra13486f

instance, phosphate, ammonium and corresponding organic monomers.[25,26] Therefore, the development of non-aromatic organic monomers substituted C-PPZs will also expand the types of biodegradable polymers particularly fitting for the fabrication of nano-carriers. However, to the best of our knowledge, though some cyclomatrix polyphosphazenes from aliphatic monomers are synthesized, most of them are in the form of bulk resin,[39–41] and there is still lack of a method for preparing their nanomaterials. The aim of this work is to explore a universal approach for preparation of polyphosphazene nanoparticles from aliphatic monomers, especially from esterified amino acid.

We have found that the substitution reaction between L-cystine methyl ester (CysM), one non-aromatic organic monomer, and HCCP stopped at the oligomer stage in a routine procedure (Scheme 1); the resultant oligomers were soluble in organic solvents because of the flexibility and good solubility of their non-aromatic side chain.[42] This resulted in the difficulties in polycondensation and thus no formation of particles. Interestingly, the oligomer solution turned cloudy when a certain amount of water was added to the oligomer solution. The existence of nanoparticles in the cloudy solution was confirmed by scanning electron microscope (SEM). This phenomenon usually appears in polymer solutions when the polymer solubility changes from good to poor.[43,44] We defined the cloudy point as lower critical solubility parameter (LCSP), *i.e.* oligomers keep stable in the solution and do not aggregate to form polymeric nanoparticles until the solubility parameter (SP) of the solution increases to this value. After aggregation, crosslinking occurs inside the aggregates *via* remaining active groups, and ultimately, sophisticated C-PPZ nanoparticles form. Although there is no direct way to determine the SP of the oligomers, this process can be estimated by the change in SP of the mixed solvent (δ_m). δ_m can be calculated by using the Hildebrand solubility parameter (δ) and volume fraction (ϕ) of the existing solvent and additional poor solvent as follows:[45]

$$\delta_m = \sum \phi_i \delta_i,\ i = 1, 2 \quad (1)$$

We have proposed a hypothesis that the formation of C-PPZ nanoparticles from aromatic or non-aromatic organic monomers obeys a unified polycondensation route (Scheme 2) that is governed by the solvent system SP. Polycondensations between aromatic monomers and HCCP in previous reports, which nucleated directly and grew further to form nanoparticles,[46,47] were merely special cases. In these cases, the SP of the reaction solvents exceeds the LCSP of the corresponding oligomers, which is lower because of monomer hydrophobicity. They therefore tended to directly aggregate to form particles (Scheme 2, blue route). In contrast, oligomers from non-aromatic monomers have a similar SP to that of the reaction solvents, are dissolvable in the reaction solution and exhibit a relatively stable behavior. Therefore, an extra driving

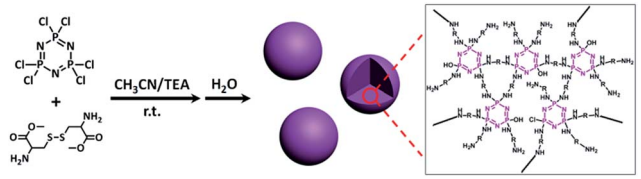

Scheme 1 Preparation process of PPZ-CysM nanoparticles from HCCP and CysM.

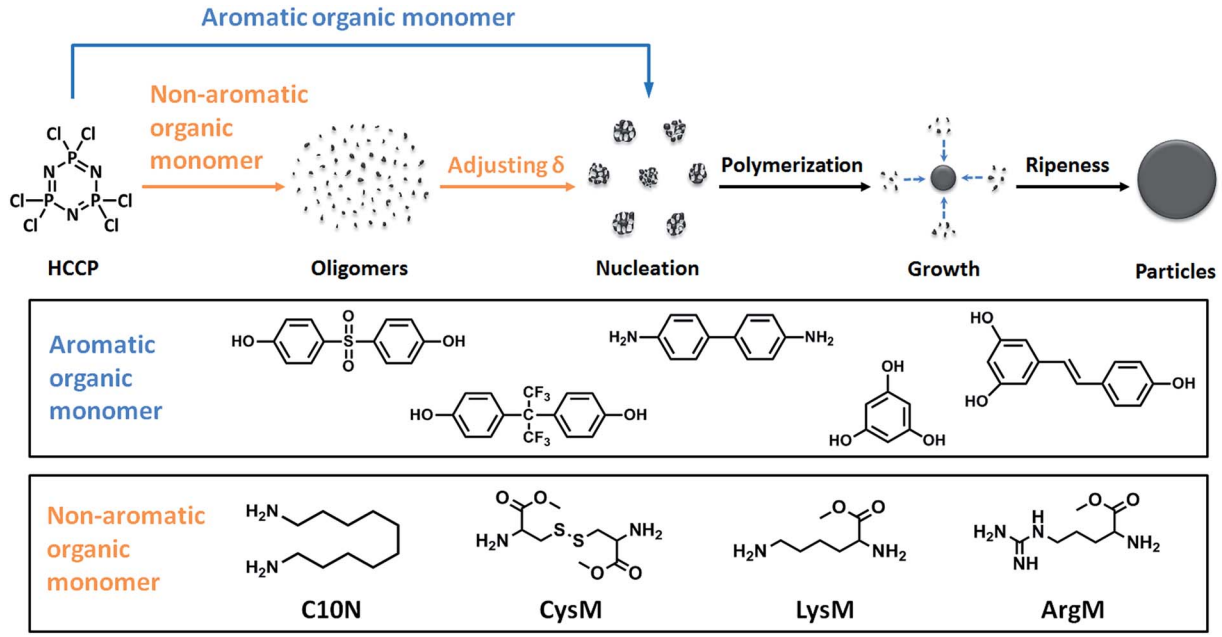

Scheme 2 Unified precipitation polycondensation route of cyclomatrix polyphosphazene nanoparticles and the typical example of aromatic and non-aromatic organic monomer used.

force provided by a poor solvent (water) is required for their aggregation (Scheme 2, orange route). We suspect that an upper critical solubility parameter (UCSP) exists, *i.e.*, where no polymeric nanoparticles would form until the δ_m were lower than this value. Therefore, we propose a new method termed solubility-parameter-triggered polycondensation with UCSP and LCSP values. We have tested this hypothesis experimentally and theoretically. 1,10-Diaminodecane (C10N), L-cystine methyl ester (CysM), L-lysine methyl ester (LysM), L-arginine methyl ester (ArgM) and a series of solvents with different SPs as summarized in Table 2 were selected for testing. Diethyl ether ($\delta = 7.4$ cal$^{0.5}$ cm$^{-1.5}$) and water ($\delta = 23.4$ cal$^{0.5}$ cm$^{-1.5}$) were chosen as the two typical poor solvents and they were used to adjust the solvent systems δ_m to a lower or higher value, respectively.

2 Experimental section

2.1 Materials

HCCP (Adamas-Beta) was recrystallized from dry hexane followed by sublimation (~0.1 MPa) twice. The melting point of the purified HCCP was 113–114 °C. C10N was purchased from Adamas-Beta, CysM, LysM, ArgM were purchased from GL Biochem Ltd. All the solid reactants were used directly. TEA was purchased from Aldrich and was used without further purification. Diethyl ether, toluene, ethyl acetate, THF, acetone, acetonitrile, ethanol and methanol were from Shanghai Chemical Reagents Corp., were dried by molecular sieve and were distilled. Water was purified to a resistivity higher than 18.2 MΩ cm using a Hitech system.

2.2 Characterization

^{1}H, ^{13}C and ^{31}P NMR spectra were recorded on a Varian Mercury Plus-400 nuclear magnetic resonance spectrometer (400 MHz). $CDCl_3$ was used as internal reference in ^{1}H and ^{13}C NMR analysis, while 85% phosphoric acid was used as external reference in ^{31}P NMR analysis. Fourier-transform infrared spectra were recorded on a Paragon 1000 (Perkin-Elmer) spectrometer. Samples were dried overnight at 45 °C under vacuum and were mixed thoroughly and crushed with KBr to produce KBr pellets. The molecular weight and polydispersity were estimated using a Waters 1515-2414 (Waters, USA) gel permeation chromatograph at 30 °C equipped with three linear mixed-B columns (Polymer Lab Corporation; pore size: 10 μm, column size: 300 × 7.5 mm) and a refractive index detector. Dimethylformamide (0.01 mol L^{-1} LiBr) and polystyrene were used as the eluent (elution rate: 1.0 mL min^{-1}) and calibration standard, respectively. Mass spectra were analyzed on a LCMS-2020 (Shimadzu) with methanol as eluent. SEM images were taken by using an FEI Nano 450 at an activation voltage of 800 V and a retarding field of 4000 V. TEM images were taken using an FEI-Tecnai G2 Spirit Biotwin operated at a 120 kV accelerating voltage. Samples were prepared on the surface of 300-mesh Formvar-carbon film-coated copper grids. The mean nanoparticle size was determined by DLS using a Malvern Nano_S instrument (Malvern, UK) at 25 °C. All measurements were repeated three times.

Table 1 The preparation formula of PPZ-CysM/PPZ-LysM/PPZ-ArgM/PPZ-C10N oligomers in a series of molar feed ratio, unit: g

Molar feed ratio	1 : 1	1 : 2	1 : 3	1 : 4	1 : 5	1 : 6
HCCP	0.50	0.50	0.50	0.50	0.50	0.50
CysM·2HCl[a]	0.53	1.06	1.59	2.12	2.66	3.19
LysM·2HCl[a]	0.33	0.67	1.01	1.34	1.67	2.01
ArgM·2HCl[a]	0.37	0.75	1.12	1.50	1.87	2.25
C10N[a]	—	—	0.74	—	—	—
TEA	1.27	1.59	1.91	2.23	2.57	2.87

[a] CysM·2HCl, LysM·2HCl, ArgM·2HCl, or C10N were used separately. PPZ-C10N is only prepared under a molar feed ratio of 1 : 3.

2.3 Preparation of oligomer solutions

The preparation of PPZ-CysM at molar feed ratio of 1 : 3 was typically described, and the formula used in the preparation of C-PPZ from other organic monomers or at other molar feed ratio was listed in Table 1. And all processes were conducted in a dry nitrogen atmosphere at room temperature.

HCCP (0.50 g, 1.43 mmol) and CysM·2HCl (1.59 g, 4.31 mmol) were added to a 50 mL round-bottom flask with 25 mL each of toluene, ethyl acetate, THF, acetone, acetonitrile, ethanol and methanol, respectively. After ultrasonic mixing for 30 min, TEA (1.91 g, 18.91 mmol) was added dropwise within 5 min. The reaction was maintained for 2 d at room temperature. The byproduct, triethylamine hydrochloride was removed by centrifugation at a speed of 10 000 rpm, and the supernatant liquor was collected and stored in a sample bottle. A small quantity of reaction solutions was removed and placed in NMR tubes, which contained a sealed capillary tube with benzene-d_6.

^{31}P NMR (162 MHz, C_6D_6) of four oligomers with a molar feed ratio of 1 : 3 was conducted as follows:

PPZ-CysM: δ 24.86 (t), 23.48 (t), 17.24 (s), 15.06 (q), 13.00 (d), 11.60 (d), 1.91 (s), −3.75 (t);

PPZ-LysM: δ 24.13 (m), 21.90 (s), 21.38 (d), 19.75 (d), 16.49 (q), 15.66–13.17 (m), 11.39–10.40 (m);

PPZ-ArgM: δ 21.83 (d), 20.57 (d), 16.84–14.74 (m), 8.12 (t), 1.76 (d), −2.73 (t), −3.85 (t), −8.71 (m);

PPZ-C10N: δ 21.90 (m), 20.65–19.72 (m), 15.06 (d), 2.48–1.50 (m), 1.06 to −1.24 (m), −3.58 to −4.41 (m), −10.24 (t).

2.4 Preparation of C-PPZ clusters or nanoparticles

As-prepared PPZ-C10N, PPZ-CysM, PPZ-LysM, and PPZ-ArgM oligomer solutions (3.0 mL) were injected separately into 10 mL centrifuge tubes. Diethyl ether or water was added dropwise to each sample, until a white solid precipitate formed. The amount of Et_2O or water was recorded and was used to calculate UCSP or LCSP by eqn (1), respectively. Precipitates were separated by centrifugation at 10 000 rpm, and were washed three times using deionized water and alcohol. The washed products were dispersed in 2 mL water, and used for DLS studies directly

or dropped onto clean silicon wafers for SEM studies. Each C-PPZ yield is listed in Table S1.†

3 Results and discussion

3.1 UCSP/LCSP of C-PPZ oligomers

Oligomers from C10N, CysM, LysM and ArgM were termed as PPZ-C10N, PPZ-CysM, PPZ-LysM and PPZ-ArgM oligomers, respectively. Toluene (δ: 8.9), ethyl acetate (δ: 9.1), tetrahydrofuran (THF, δ: 9.9), acetone (δ: 10.0), acetonitrile (δ: 11.9), ethanol (δ: 12.7) and methanol (δ: 14.5) were chosen as reaction solvents, as they can dissolve reactants (except ArgM in toluene). Triethylamine (TEA) was used as an acid-binding agent, and the resultant byproduct, triethylamine hydrochloride, was removed by centrifugation before addition of poor solvent. Samples were taken from the supernatants for nuclear magnetic resonance (NMR) analysis. The ^{1}H, ^{13}C and ^{31}P NMR spectra (Fig. S1a–d†) of the supernatants showed that the reactions occurred between HCCP and the four non-aromatic organic monomers; however, all products obtained were mixtures.[48] Gel permeation chromatograph (GPC) analyses (Fig. S2†) showed that the molecular weights of all products were lower than 5000 Da, which means that only oligomers with a small molecular weights were formed during polymerization. MS results of the four supernatants (Fig. S3†) further show that these oligomers are composed of multi-substituted mixtures. The stable existence of these oligomers in the solvent results because of their SPs matching those of the solvents; in this case, the solvation layer can surround the oligomers, and the solvation effect (Fig. 1a) is crucial for the oligomer stability.[49] When water with a high δ value or diethyl ether (Et_2O) with a low δ value were added into the oligomer solution, the δ_m deviated from the oligomer SP. Once δ_m decreases or increases to a certain value (*i.e.*, UCSP or LCSP), the surrounding solvation layer breaks, the oligomers aggregate and polycondensation occurs (Fig. 1b), and C-PPZ nanoparticles are formed. Critical points of δ_m, at which the reaction mixture changes from transparent to cloudy, are termed UCSP and LCSP, respectively. The process to prepare C-PPZ nanoparticles is defined the solubility-parameter-triggered polycondensation. Table 2 lists UCSP (italics) and LCSP (**bold**) values of a series of oligomers measured in several solvents by Et_2O or H_2O addition. *In situ*-formed byproduct trimethylamine hydrochloride disturbed the determination of the cloud point, when Et_2O was added in oligomer solutions with acetone, acetonitrile, ethanol or methanol as solvents. Therefore, the UCSPs of oligomers in these solvents were not provided. Water is immiscible with toluene and ethyl acetate and so the LCSPs of oligomers in these solvents also could not be detected. Although the values of UCSP and LCSP vary from oligomer to oligomer, they are almost constant (see the last row in Table 2) and are independent of oligomer solvents. Each oligomer should therefore possess a unique solubility parameter, which will be calculated later. When the δ_m of the mixture solvent varies between UCSP and LCSP, the oligomer is quite stable in solution. However, aggregation occurs immediately once the δ_m is lower than the UCSP or higher than the LCSP. A stronger substituted organic monomer hydrophobicity (hydrophobicity sequence: C10N > CysM > LysM > ArgM) results in a lower UCSP and LCSP (discussed later in Fig. 6a). Therefore, the fact that the C-PPZs derived from aromatic organic monomers underwent direct polycondensation and deposition from solvent (acetonitrile, THF or acetone) as reported previously, should be ascribed to the low solubility parameter of their oligomers because of the high hydrophobicity of their organic monomers. The δ values of the solvents used should exceed the LCSP and therefore the C-PPZ nanoparticles from 4,4′-sulfonyldiphenol and HCCP can form nanoparticles directly even in toluene with a low δ (8.9). C-PPZ nanoparticle formation from ArgM and HCCP, which also undergo direct polycondensation in toluene, is different because the δ of toluene (8.9) is slightly lower than the UCSP of the PPZ-ArgM oligomer, and precipitation polycondensation can occur directly.

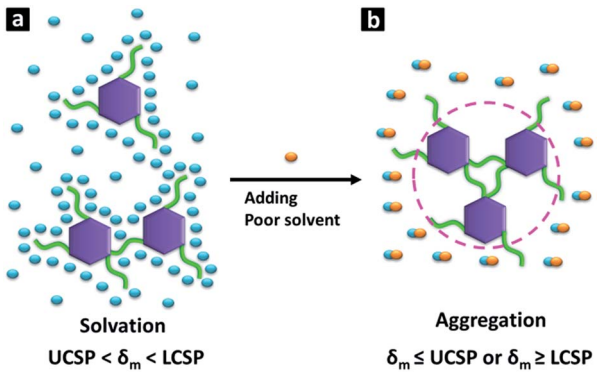

Fig. 1 (a) Oligomer solvation by solvent molecules when the δ_m is between UCSP and LCSP. After poor solvent addition, (b) desolvation and oligomers aggregation occurs when $\delta_m \leq$ UCSP, or $\geq$ LCSP.

3.2 Formation mechanism of nanoparticles

To understand the mechanism of the solubility-parameter-triggered polycondensation, we followed the formation of C-PPZ nanoparticles using HCCP–CysM oligomers as a sample and THF as solvent. Triethylamine hydrochloride byproduct was removed from the reaction mixture of CysM and HCCP. Oligomer diameter analysis was carried out by dynamic light scattering (DLS) and transmission electron microscopy (TEM), oligomers of 7 nm were detected (inset in Fig. 2). As mentioned above, the oligomers could exist in the solvent because of solvation effect. When Et_2O or water was added continuously into the oligomer solution, the oligomer diameter remained unchanged until the δ_m reached the UCSP or LCSP value of the oligomers. Photographs of the particles in solutions before and after reaching close to the UCSP or LCSP point were taken by SEM as shown in Fig. 2. Clusters or nanoparticles formed when the δ_m was lower than the USCP or exceeded the LCSP, respectively. Interestingly, the nanoparticle diameter no longer changes with increase in water once formed. Based on these experimental results, we summarize and illustrate the nanoparticle formation process in Fig. 3. The UCSP to LCSP range is the stable region of the C-PPZ oligomers. In this region, oligomers can occur at a high concentration, for example, the weight

Table 2 UCSP (*italics*) and the LCSP (**bold**) of the four organic monomers respectively substituted oligomer in a series of solvents

	Oligomers and their corresponding UCSP and LCSP value obtained in different solvents[a]							
Solvent (δ)	PPZ-C10N		PPZ-CysM		PPZ-LysM		PPZ-ArgM	
Toluene (8.9)	*8.25*	—[b]	*8.49*	—[b]	*8.73*	—[b]	*NPs*[d]	—[b]
Ethyl acetate (9.1)	*8.25*	—[b]	*8.53*	—[b]	*8.76*	—[b]	*8.91*	—[b]
Tetrahydrofuran (9.9)	*8.23*	**15.69**	*8.51*	**18.09**	*8.83*	**19.25**	*9.06*	**20.70**
Acetone (10.0)	—[c]	**15.74**	—[c]	**18.14**	—[c]	**19.28**	—[c]	**20.72**
Acetonitrile (11.9)	—[c]	**15.73**	—[c]	**18.19**	—[c]	**19.22**	—[c]	**20.69**
Ethanol (12.7)	—[c]	**15.62**	—[c]	**18.05**	—[c]	**19.12**	—[c]	**20.73**
Methanol (14.5)	—[c]	**15.49**	—[c]	**17.92**	—[c]	**19.21**	—[c]	**20.66**
Mean values of *UCSP*/**LCSP**	*8.24*	**15.58**	*8.51*	**18.08**	*8.77*	**19.16**	*8.99*	**20.70**

[a] Ratio of HCCP to amino acid ester is 1 : 3. Et_2O or H_2O (poor solvent) added to determine the UCSP or LCSP, respectively. [b] Solvents are immiscible with water. [c] Byproduct triethylamine hydrochloride interferes with assessment of UCSP. [d] Precipitation polycondensation occurred.

percentage of PPZ-CysM oligomer can reach as high as 80% in anhydrous acetonitrile. However, the C-PPZs oligomer aggregation occurs once the δ_m value is equal or lower than UCSP, or equal or higher than LCSP. Fig. 3, S4 and S5† show that the product morphologies obtained by the two pathways differ, the aggregates triggered by Et_2O (δ_m < UCSP) almost form clusters, whereas those triggered by water (δ_m > LCSP) are almost nanoparticles. The morphology difference may be caused by the hydrophobic–hydrophilic balance between oligomers and solvents. Polyphosphazenes are considered to be hydrophobic, once the solvation layer outside of the oligomers is peeled, the oligomers immediately gather together because of hydrophobic interaction, and further deeply polycondensation occurs between residual active groups inside the particles. Because the hydrophobic interaction is stronger in the presence of water, a greater compressive force is exerted on the aggregates, which makes the resulting particles more rigid, and elastic collision between particles make it more difficult to stack. In contrast, the aggregates obtained in the presence of Et_2O are relatively soft; a certain degree of sticking thus occurs between primary particles, which leads to the formation of clusters.

In FT-IR spectra (Fig. 4), the peaks at 2908 and 2841 cm^{-1} are assigned to stretching vibration of $-CH_2-$ groups on C10N, 1740 cm^{-1} refers to the stretching vibration of C=O on amino acid esters, 1215 cm^{-1} refers to the stretching vibration of P=N on the cyclotriphosphazene ring, indicating that these nanoparticles derived from cyclotriphosphazene group and corresponding organic monomers. The precipitates (*e.g.* PPZ-CysM nanoparticles) have no glass-transition temperature (Fig. S6a†), but an obvious increase in the onset of the thermal-degradation (T_d) temperature (Fig. S6b†), implying that the polymer particles consist of cross-linked structure.

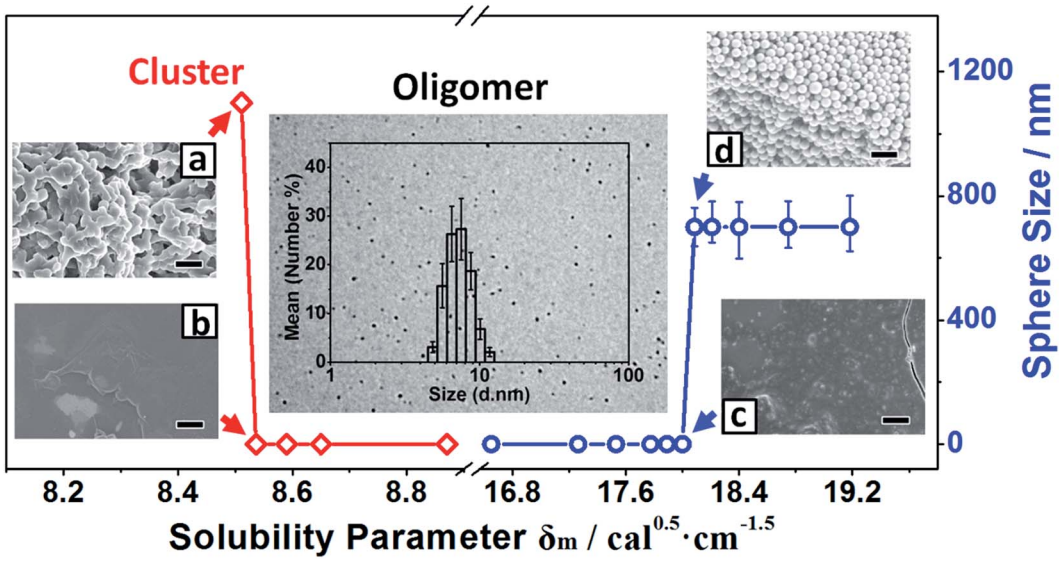

Fig. 2 Hildebrand solubility parameter of the mixed solvent (δ_m) and its relationship with PPZ-CysM sphere size. Sphere growth does not occur when δ_m value varies from 8.54 $cal^{0.5}$ $cm^{-1.5}$ (point b, Et_2O/THF is 24/20) to 18.00 $cal^{0.5}$ $cm^{-1.5}$ (point c, water/THF is 30/20). Clusters (of uncountable size) are formed when δ_m is lower than 8.51 $cal^{0.5}$ $cm^{-1.5}$ (point a, Et_2O/THF is 25/20), whereas spheres are formed when δ_m value is larger than 18.09 $cal^{0.5}$ $cm^{-1.5}$ (point d, water/THF is 31/20). Greater δ_m values results in more rapid growth, with little effect on sphere size. The scale bar is 2 μm.

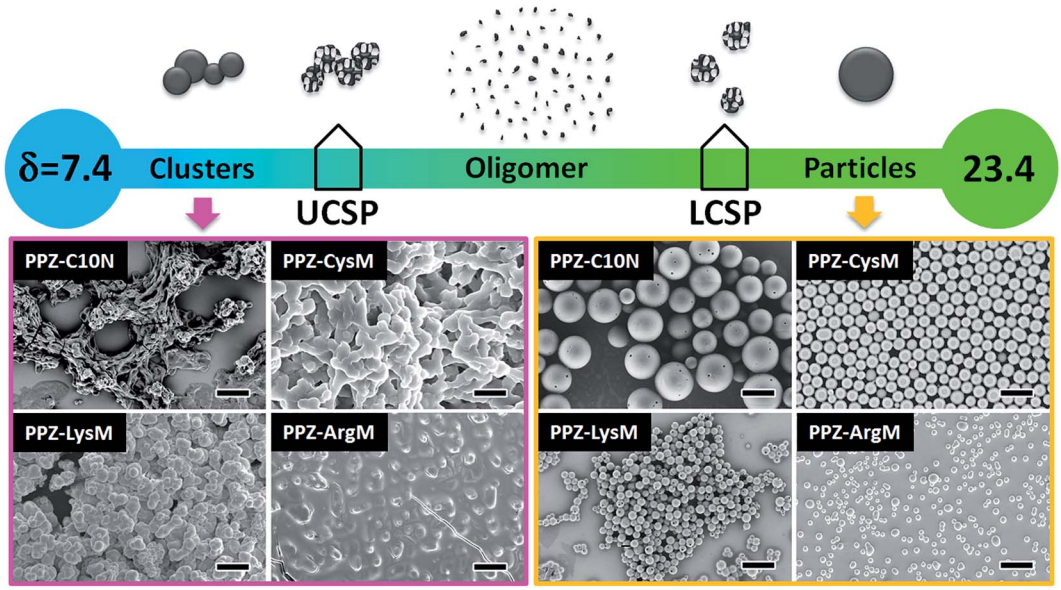

Fig. 3 SP regions and corresponding C-PPZ morphologies. SEM images were selected from Fig. S4 and S5† and show the C-PPZ precipitate morphologies of the C-PPZ precipitates prepared at a δ_m lower than UCSP (left, purple border) or higher than LCSP (right, yellow border). 7.4 and 23.4 refer to the SP value of Et_2O and H_2O, respectively. Scale bar is 2 μm.

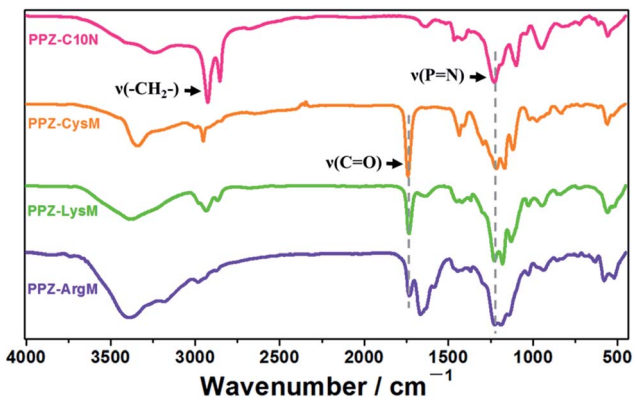

Fig. 4 IR analysis of PPZ-C10N (red), PPZ-CysM (orange), PPZ-LysM (green), PPZ-ArgM particles (violet).

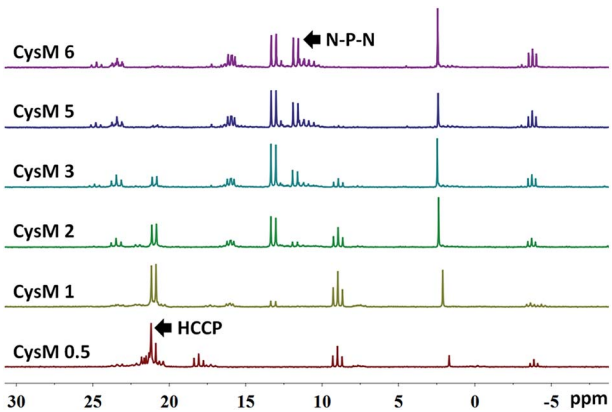

Fig. 5 ^{31}P NMR studies of PPZ-CysM oligomers with different CysM molar feed ratio.

3.3 Influence of molar feed ratio on UCSP/LCSP

The oligomer UCSP/LCSP is determined by monomer hydrophobicity and is also influenced by the molar feed ratio, which adjusts the oligomer hydrophobicity. A higher molar feed ratio of amino acid esters results in greater amino acid ester substitution (as shown in Fig. S8a and b†). We used ^{31}P NMR with PPZ-CysM as an example to illustrate qualitatively the substitution rate of CysM on HCCP. ^{31}P NMR studies (Fig. 5) of PPZ-CysM oligomers with different CysM molar feed ratios (HCCP : CysM = 1 : x, termed CysM x, where x = 0.5–6) confirm that the increase in amount fed strengthens the signal intensity of the [N–P–N] moiety, which results in an increased substitution of amino acid ester on the HCCP.[21] Different substitution rates of amino acid esters vary the UCSP/LCSP of the C-PPZ oligomers. The UCSP/LCSP of three kinds of amino acid ester-substituted C-PPZ oligomers were tested quantitatively. According to Fig. 6a, the UCSP and LCSP values of the three kinds of amino acid ester-substituted C-PPZs increase with increase in molar feed ratio. That occurs because the amino acid ester substitution decreases the oligomer hydrophobicity and results in less Et_2O or more water required to facilitate oligomer aggregation. For the same molar feed ratio, the oligomers from amino acid ester with a higher hydrophilicity have a higher UCSP/LCSP. Phase diagrams of PPZ-CysM, PPZ-LysM and PPZ-ArgM oligomers are shown in Fig. 6b–d. For PPZ-CysM oligomer, it keeps stable in the solution when the δ_m of solvent system is between its UCSP and LCSP (Phase I, oligomer area), and aggregate to form particles or clusters when the δ_m is higher than LCSP (Phase II, particle area) or lower than UCSP (Phase III, cluster area). While for PPZ-LysM or PPZ-ArgM

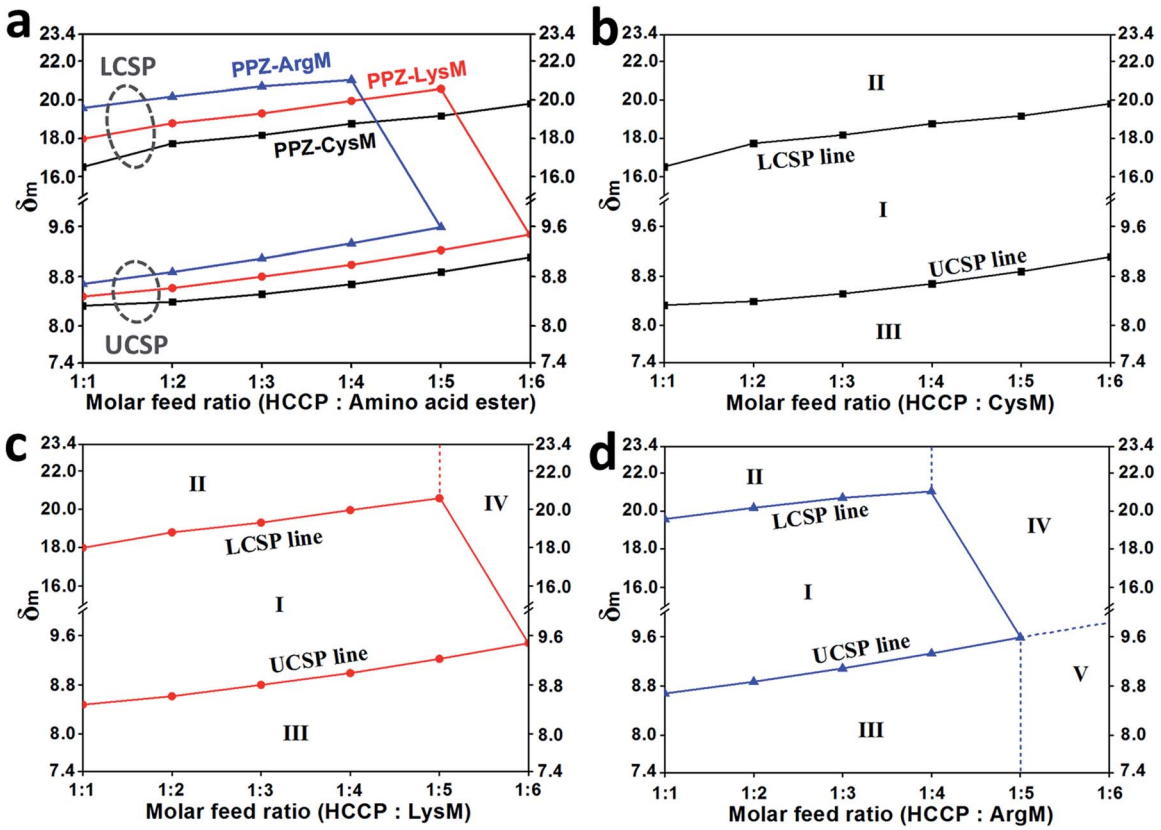

Fig. 6 Phase diagrams of (a) PPZ-CysM, (b) PPZ-LysM and (c) PPZ-ArgM. Phase I: water triggerable oligomer area, Phase II: particles area, Phase III: clusters area, Phase IV: water non-triggerable oligomer area, Phase V: direct precipitation polymerization area. Dashed line refers to extended auxiliary line. (d) Comparing the changes of UCSP and LCSP of PPZ-CysM, PPZ-LysM and PPZ-ArgM oligomers with increase in molar feed ratio of HCCP to corresponding amino acid esters.

oligomers, when their molar feed ratio is higher than 1 : 5 or higher than 1 : 4, respectively, it is failed to trigger the formation of any precipitation by water. This is because the higher hydrophilicity makes the oligomer soluble in water, then we name Phase IV water non-triggerable oligomer area. Furthermore, when the molar feed ratio of PPZ-ArgM oligomer is higher than 1 : 5 and a low SP solvent is used, precipitation polymerization between HCCP and ArgM happens directly to form clusters (Phase V), as the δ_m of the reaction solvent is lower than the UCSP of the corresponding oligomer.

3.4 Influence of molar feed ratio on nanoparticle size and yield

Change of amino acid ester feed ratio can affect oligomer hydrophilicity and LCSP, which determines the nanoparticle formation of C-PPZ oligomers. Therefore, the size and yield of C-PPZ nanoparticles are speculated to be variable for different molar feed ratios. DLS was used to determine the C-PPZ nanoparticle diameter. The Z-average diameter of C-PPZ nanoparticles (S9a–c) is summarized in Fig. S9d.† For the same molar feed ratio, C-PPZ nanoparticles from amino acid ester with a higher hydrophilicity present a relatively smaller diameter (size order: PPZ-ArgM < PPZ-LysM < PPZ-CysM). We also tested the yield of precipitated C-PPZ nanoparticles by weighing as shown in Fig. S9e.† The trend in nanoparticle yield against oligomer hydrophilicity agrees with that of its diameter against oligomer hydrophilicity. This occurs because of the higher hydrophilicity that enhances the oligomer dissolvability in water, leads to some remnant oligomers in mixed solvent during water-triggered precipitation polycondensation and results in a lower yield. The smaller size is caused by a decrease in nucleation and growth ability of the oligomers because of the increase in hydrophilicity. The nanoparticle diameter and yield is also dependent on the molar feed ratio. Diameter and yield decrease with increase in molar feed ratio. The result can also be explained by the hydrophilicity, namely, the higher molar feed ratio creates a higher substitution of amino acid ester on HCCP and increases the C-PPZ oligomer hydrophilicity, which leads to an enhanced oligomer solubility in mixed solvent and a reduced ability for nucleation and growth. When the molar feed ratio is higher than 1 : 4, the PPZ-ArgM oligomers cannot form precipitated nanoparticles during the water-triggered process.

3.5 Degradability and biocompatibility of PPZ-CysM nanoparticles

The as-prepared PPZ-CysM nanoparticles underwent gradual degradation in deionized water under 37 °C and became

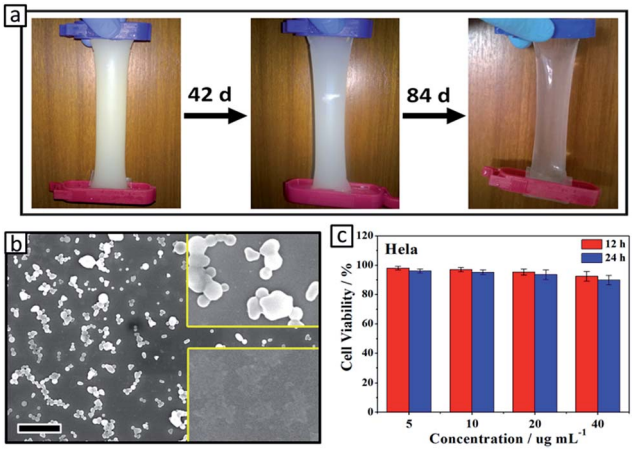

Fig. 7 (a) Degradability property of PPZ-CysM nanoparticles at 37 °C in deionized water. (b) SEM analysis of hydrolyzed PPZ-CysM nanoparticles. (c) Cell viability study of PPZ-CysM nanoparticles.

a transparent solution after 84 days (as shown in Fig. 7a). SEM study (Fig. 7b) also reveals the size of particles decreased obviously over time until complete disappearance (insert at lower right corner). HeLa cells were incubated in PBS buffer containing PPZ-CysM nanoparticles with different concentrations. All cell viabilities were above 90% (Fig. 7c) after incubation for 24 h, indicating the nanoparticles were of biologically low cytotoxicity. Further study on its bioapplication is in progress.

3.6 Computational simulations

The oligomer stability in a solvent system within UCSP and LCSP is regarded as the binary system miscibility, *i.e.*, the oligomer–solvent pair is miscible. The Flory–Huggins interaction parameter χ is the determining factor. It describes the strength of a specific pair of solvent–solute interactions and controls the solubility of this pair at a given temperature, *i.e.*, the smaller χ value is, the more miscible the binary system becomes. The interaction parameter is calculated from:

$$\chi = \frac{V_{ref}}{kT}\frac{\Delta H_m}{V_m}\frac{1}{\emptyset_s \emptyset_p} \quad (2)$$

This takes into account the specific interaction between oligomers and the solvent system, whereas we consider the mixed solvent to be a unique system. To obtain an insight into the oligomer miscibility with the solvent system (in this case, we focused on PPZ-CysM oligomers and on the acetonitrile/water solvent system) on molecular level, we performed multi-sample molecular dynamics (MD) calculations[50] on the solubility properties of the oligomer/solvent systems.

The model structure for oligomer presented in Fig. S11c† was built based on our experimental observation, *i.e.*, the detected oligomers were mainly substituted monomers and dimers with 33% unreacted chlorine on a HCCP ring.[42] The geometry of the model structure was also supported by the reported crystal structure of similar HCCP compounds[51,52] and our computational results (details see ESI S12†).

Table 3 Sampling effects on the oligomer properties using the NPT[a]-MD simulation

	Sample size	Atom number	δ_s (cal mL^{-1})^0.5	ρ (g mL^{-1})
Monomer	1	132	9.63	1.385
	5	660	9.71	1.380
Dimer	1	232	8.90	1.379
	5	1160	9.22	1.380

[a] The isothermal–isobaric ensemble (NPT ensemble).

The Hildebrand SPs for pure oligomers and solvent systems were estimated by MD calculation. The computer simulated SPs of mixed solvents δ_s (Fig. S13,† -▲-) has, a similar trend as that (δ_m) calculated according to eqn (1), *i.e.*, the experimental trend (Fig. S13,† -●-). Slight larger δ_s values could contribute to the specific interactions between water and acetonitrile molecules, which is ignored in eqn (1). Because of the lack of available experimental values, we only compared the computed density (ρ) (the overall molecular weight in a fixed volume of the amorphous cell) and SP (δ_s) between models with different sizes for PPZ-CysM oligomers (Table 3). There is no significant difference in density between the two sizes, whereas the SPs increase slightly when the boundary system increases. The SPs calculated for all systems fit into the solubility gap between UCSP and LCSP.

We also considered oligomers immersed in mixed solvents (example model see Fig. S14†) to study their solubility properties. No significant difference between monomer and dimer were found, thus we used the monomer model in the following study to reduce the computational time. A curve of the computed χ *versus* SPs of the mixed solvents is shown in Fig. 8. It matches the trends presenting in Fig. 2. The variation of interaction parameters could be neglected when the SP was below 17.89 cal$^{0.5}$ cm$^{-1.5}$, and then it increased slightly at 18.01 cal$^{0.5}$ cm$^{-1.5}$. Beyond this point, χ increased significantly by 36% when the solubility parameter increased to 18.11 cal$^{0.5}$ cm$^{-1.5}$ and remained almost constant afterwards. We noticed that the simulated LCSP value is slightly lower than the experimental value of 18.20 cal$^{0.5}$ cm$^{-1.5}$. For a modeled system, a MD

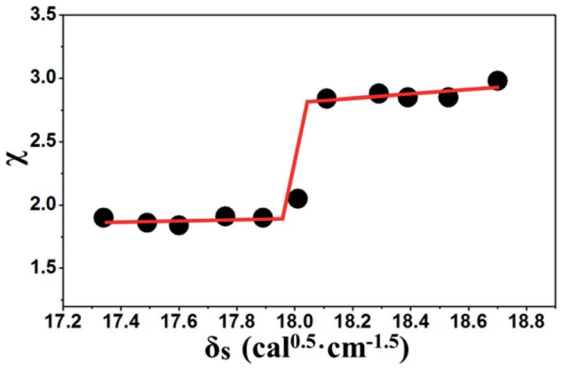

Fig. 8 Interaction parameter for oligomer-mixed solvent pairs.

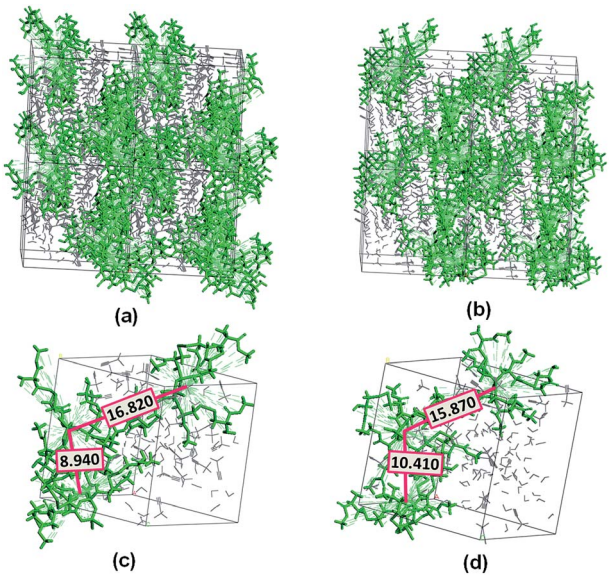

Fig. 9 Amorphous cell packed with 3 oligomer molecules and 100 solvent molecules (volume ratio of water to acetonitrile is 0.86). (a) and (b) present a 2 × 2 × 2 super cell before and after MD runs, respectively. (c) and (d) present a unit cell before and after MD runs. Unit: Å.

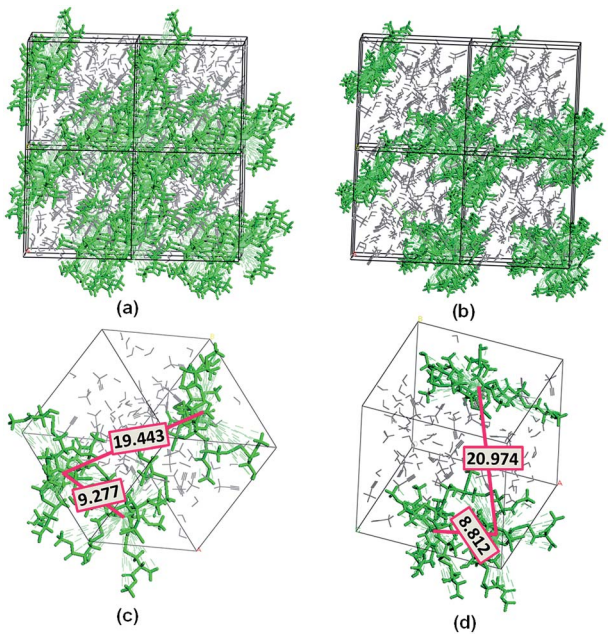

Fig. 10 Amorphous cell packed with 3 oligomer molecules and 100 solvent molecules (volume ratio of water to acetonitrile is 0.86). (a) and (b) present a 2 × 2 × 2 super cell before and after MD runs, respectively. (c) and (d) present a unit cell before and after MD runs.

simulation is performed until the entire system reaches equilibrium, whereas in experimental work, the determination of solvent solubility is non-trivial and measurements are affected by a sizable uncertainty. For example, water was added to the acetonitrile solution of PPZ-CysM until a white solid formed and this was determined visually. Water already tends to excess when the polymerization is observed, and thus leads to a slightly higher SP than its theoretical value obtained after the system was fully equilibrated.

To investigate the effect of solvent solubility on oligomer distribution, we used two systems that contain three oligomer molecules and a mixed solvent with volume ratios (water to acetonitrile) of 0.86 and 1.17, respectively. These correspond to an oligomer solution below and beyond the LCSP point. After optimization, MD simulations of each system were run until the volume and energy had equilibrated. Fig. 9 shows that when the volume ratio is 0.86 (SP is 17.49 $cal^{0.5}$ $cm^{-1.5}$), the oligomer molecule distribution did not change significantly before and after the MD run (a and b). Two oligomers were packed close initially with an intermolecular distance of 8.94 Å Fig. 9(c) (the distance was measured from the center of one oligomer molecule to the center of another molecule). After a MD run of 400 ps, the two oligomers were separated by 2 Å, which indicates that no aggregation occurred in this solution.

When the volume ratio reaches 1.17, *i.e.*, the solvent SP is 18.29 $cal^{0.5}$ $cm^{-1.5}$, the oligomer aggregation in the system is obvious (Fig. 10a and b). Three oligomers, two in the same unit cell with an initial distance of 9.277 Å (Fig. 10c), and a third one in the neighbor cell, moved together to form a cluster (Fig. 10d). The distance between the two oligomer in one cell was shortened to 8.812 Å. This agrees with our experimental results, *i.e.*, the oligomer aggregation to form clusters was observed when a SP reached LCSP (18.2 $cal^{0.5}$ $cm^{-1.5}$).

4 Conclusions

Solubility-parameter-triggered precipitation polycondensation was proposed to prepare C-PPZs nanoparticles from non-aromatic monomers. Two important critical parameters, involving UCSP and LCSP, were found to be boundary-lines. We demonstrated experimentally and computationally that the reactions between HCCP and non-aromatic organic monomers form oligomers, which can be stable in solvent if the SPs of their solutions are within the UCSP and LCSP range. Conversely, crosslinked polymeric particles can be precipitated from solutions. Corresponding UCSP/LCSP values are fixed for a given organic monomer structure and its molar feed ratio, which allows for the prediction of the most optimal SP for C-PPZ preparation. More importantly, based on this demonstration, organic monomers with two reactive groups, no matter aromatic or not, could be used to synthesize various C-PPZs, which creates a species of novel biomaterials.

Acknowledgements

This work was supported by the Major Project of Chinese National Programs for Fundamental Research and Development (973 Project: 2012CB933803 and 2014CB643605), and the National Science Foundation of China (grant No. 51573089).

References

1 L. Meng, C. Xu, T. Liu, H. Li, Q. Lu and J. Long, *Polym. Chem.*, 2015, **6**, 3155.

2 J. L. Nichol and H. R. Allcock, *Eur. Polym. J.*, 2015, **62**, 214.
3 L. S. Nair and C. T. Laurencin, *Prog. Polym. Sci.*, 2007, **32**, 7628.
4 M. Deng, S. G. Kumbar, Y. Wan, U. S. Toti, H. R. Allcock and C. T. Laurencin, *Soft Matter*, 2010, **6**, 3119.
5 Y. M. Bi, X. Y. Gong, W. Z. Wang, L. Yu, M. Q. Hu and L. D. Shao, *Chin. Chem. Lett.*, 2010, **21**, 237.
6 J. Fan, H. Zhu, R. Li, N. Chen and K. Han, *J. Mater. Chem. A*, 2014, **2**, 8376.
7 M. l. He, H. l. Xu, Y. Dong, J. H. Xiao, P. Liu, F. Y. Fu, S. Hussain, S. Z. Zhang, C. J. Jing and Q. Yu, *Chin. J. Polym. Sci.*, 2014, **32**, 151.
8 S. Jankowsky, M. Hiller and H.-D. Wiemhöfer, *J. Power Sources*, 2014, **253**, 256.
9 S. Jankowsky, M. Hiller, R. Stolina and H. D. Wiemhöfer, *J. Power Sources*, 2015, **273**, 574.
10 J. Bartels, A. Hess, H.-S. Shiau, H. R. Allcock, R. H. Colby and J. Runt, *Macromolecules*, 2014, **48**, 111.
11 D. He, S. Y. Cho, D. W. Kim, C. Lee and Y. Kang, *Macromolecules*, 2012, **45**, 7931.
12 M. Wang, J. Fu, D. Huang, C. Zhang and Q. Xu, *Nanoscale*, 2013, **5**, 7913.
13 J. Qian, W. Wei, X. Huang, Y. Tao, K. Chen and X. Tang, *J. Power Sources*, 2012, **210**, 345–349.
14 X. Huang, W. Wei, X. Zhao and X. Tang, *Chem. Commun.*, 2010, **46**, 8848.
15 Y. Brahmi, N. Katir, M. Ianchuk, V. Collière, E. M. Essassi, A. Ouali, A.-M. Caminade, M. Bousmina, J. P. Majoral and A. El Kadib, *Nanoscale*, 2013, **5**, 2850.
16 R. A. Dubois, P. E. Garrou, K. D. Lavin and H. R. Allcock, *Organometallics*, 1986, **5**, 460–466.
17 A. Zhang, Y. Bian, J. Wang, K. Chen, C. Dong and J. Ren, *Nanoscale*, 2016, **8**, 5006.
18 S. Chen, X. Lu, Z. Huang and Q. Lu, *Chem. Commun.*, 2015, **51**, 5698.
19 T. Mayer-Gall, D. Knittel, J. S. Gutmann and K. Opwis, *ACS Appl. Mater. Interfaces*, 2015, **7**, 9349.
20 X. Mu, B. Yuan, W. Hu, S. Qiu, L. Song and Y. Hu, *RSC Adv.*, 2015, **5**, 76068.
21 C. Chen, X. Liu, Z. Tian and H. R. Allcock, *Macromolecules*, 2012, **45**, 9085.
22 T. Modzelewski, N. M. Wonderling and H. R. Allcock, *Macromolecules*, 2015, **48**, 4882.
23 H. R. Allcock, *Soft Matter*, 2012, **8**, 7521.
24 M. Gleria and R. De Jaeger, *Phosphazenes: a worldwide insight*, Nova Publishers, 2004.
25 A. K. Andrianov, *Polyphosphazenes for Biomedical Applications*, Wiley, 2009.
26 H. R. Allcock and N. L. Morozowich, *Polym. Chem.*, 2012, **3**, 578.
27 H. R. Allcock, *Chemistry and Applications of Polyphosphazenes*, John Wiley & Sons, Hoboken, NJ, 2003.
28 H. R. Allcock, C. A. Crane, C. T. Morrissey, J. M. Nelson, S. D. Reeves, C. H. Honeyman and I. Manners, *Macromolecules*, 1996, **29**, 7740.
29 B. Wang, E. Rivard and I. Manners, *Inorg. Chem.*, 2002, **41**, 1690.
30 I. Teasdale, S. Wilfert, I. Nischang and O. Brüggemann, *Polym. Chem.*, 2011, **2**, 828.
31 J. H. Steinke, B. W. Greenland, S. Johns, M. P. Parker, R. C. Atkinson, I. A. Cade, P. Golding and S. J. Trussell, *ACS Macro Lett.*, 2014, **3**, 548.
32 L. Zhu, Y. Xu, W. Yuan, J. Xi, X. Huang, X. Tang and S. Zheng, *Adv. Mater.*, 2006, **18**, 2997.
33 J. Fu, Q. Xu, J. Chen, Z. Chen, X. Huang and X. Tang, *Chem. Commun.*, 2010, **46**, 6563.
34 J. Zhou, L. Meng, X. Feng, X. Zhang and Q. Lu, *Angew. Chem., Int. Ed.*, 2010, **49**, 8476.
35 W. Wei, X. Huang, X. Zhao, P. Zhang and X. Tang, *Chem. Commun.*, 2010, **46**, 487.
36 W. Wei, X. Huang, K. Chen, Y. Tao and X. Tang, *RSC Adv.*, 2012, **2**, 3765.
37 W. Wei, R. Lu, H. Xie, Y. Zhang, X. Bai, L. Gu, R. Da and X. Liu, *J. Mater. Chem. A*, 2015, **3**, 4314.
38 J. Köhler, S. Kühl, H. Keul, M. Möller and A. Pich, *J. Polym. Sci., Part A: Polym. Chem.*, 2014, **52**, 527.
39 H. Allcock, *Phosphorus-nitrogen compounds: cyclic, linear, and high polymeric systems*, Elsevier, 2012.
40 S. Krishnamurthy, K. Ramachandran, A. V. Murthy, R. A. Shaw and M. Woods, *J. Chem. Soc., Dalton Trans.*, 1980, **5**, 840.
41 J. Sun, Z. Yu, X. Wang and D. Wu, *ACS Sustainable Chem. Eng.*, 2013, **2**, 231.
42 Z. Huang, S. Chen, X. Lu and Q. Lu, *Chem. Commun.*, 2015, **51**, 8373.
43 K. Motoyoshi, A. Tajima, T. Higuchi, H. Yabu and M. Shimomura, *Soft Matter*, 2010, **6**, 1253.
44 H. Yabu, A. Tajima, T. Higuchi and M. Shimomura, *Chem. Commun.*, 2008, **38**, 4588.
45 J. Hildebrand and R. Scott, *Solubility of nonelectrolytes*, Reinhold, New York, 1950.
46 Y. Hu, L. Meng, L. Niu and Q. Lu, *Langmuir*, 2013, **29**, 9156.
47 Y. Hu, L. Meng and Q. Lu, *Langmuir*, 2014, **30**, 4458.
48 S. Ganapathiappan and S. S. Krishnamurthy, *J. Chem. Soc., Dalton Trans.*, 1987, **3**, 579.
49 S. R. Raghavan, H. Walls and S. A. Khan, *Langmuir*, 2000, **16**, 7920.
50 M. Belmares, M. Blanco, W. Goddard, R. Ross, G. Caldwell, S. H. Chou, J. Pham, P. Olofson and C. Thomas, *J. Comput. Chem.*, 2004, **25**, 1814.
51 A. Uslu, Ş. Ş. Ün, A. Kılıç, Ş. Yılmaz, F. Yuksel and F. Hacıvelioğlu, *Inorg. Chim. Acta*, 2013, **405**, 140.
52 G. Y. Çiftçi, E. Şenkuytu, M. Durmuş, F. Yuksel and A. Kılıç, *Inorg. Chim. Acta*, 2014, **423**, 489.